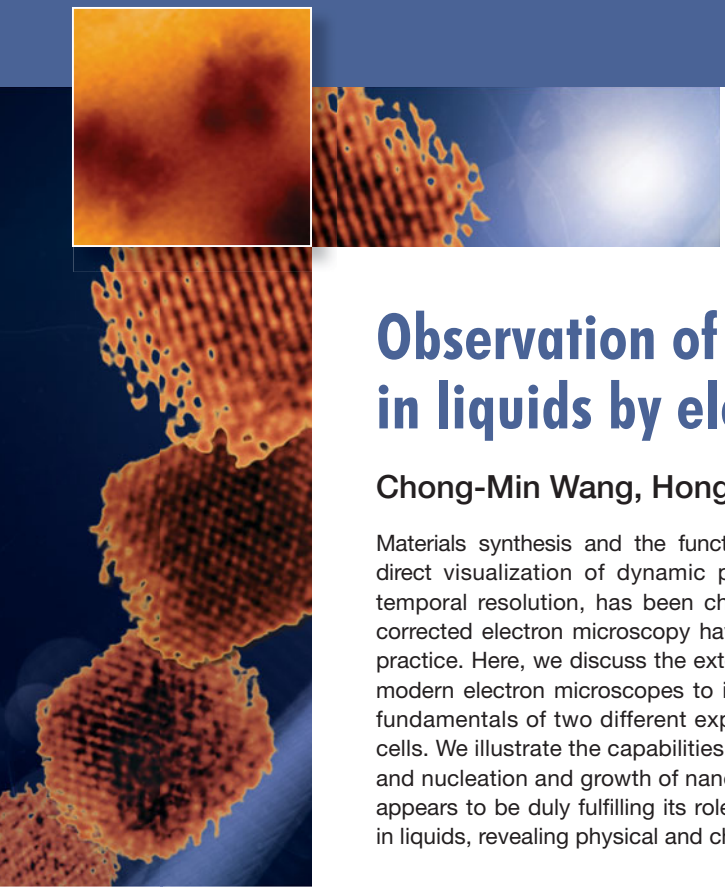


Observation of materials processes in liquids by electron microscopy

Chong-Min Wang, Hong-Gang Liao, and Frances M. Ross

Materials synthesis and the functioning of devices often involve liquid media. However, direct visualization of dynamic processes in liquids, especially with high spatial and temporal resolution, has been challenging. For solid materials, advances in aberration-corrected electron microscopy have made observations of atomic-level features a routine practice. Here, we discuss the extent to which one can take advantage of the resolution of modern electron microscopes to image phenomena occurring in liquids. We describe the fundamentals of two different experimental approaches that use closed and open liquid cells. We illustrate the capabilities of each approach by considering processes in batteries and nucleation and growth of nanoparticles from solution. Liquid-cell electron microscopy appears to be duly fulfilling its role and promise for *in situ* studies of nanoscale processes in liquids, revealing physical and chemical processes that are otherwise difficult to observe.

Introduction

Recent advances in aberration-corrected scanning/transmission electron microscopy (S/TEM) have made imaging and spectroscopy with atomic-scale resolution routine.[1–3] Concurrent with this progress is an effort to image materials at or near realistic reaction conditions. This is exemplified by *in situ* TEM observations of nanostructured material growth (such as silicon nanowire growth),[4,5] solid–gas reactions during catalysis (such as gold nanoparticles in carbon monoxide),[6–8] and materials deformation (such as nanoindentation of aluminum).[9] Such results have required both the development of dedicated microscopes that can handle gas environments around the sample (environmental TEM) and the ability to manipulate and fabricate materials at the nanoscale. The recent development of "liquid cells" for imaging liquid samples provides unique additional opportunities for understanding structure and chemical or physical processes involving materials synthesis and device functionality. Liquid-cell microscopy has been used to examine nucleation, growth, coalescence, and motion of nanoparticles in solution;[10–13] electrochemically driven processes such as deposition, corrosion, and the motion of ions;[14–17] bubble formation;[18,19] biomineralization;[20] soft materials;[21,22] and whole cells and macromolecular complexes in aqueous environments.[23–25] Its high spatial and temporal resolution, as well as its compatibility with established analytical microscopy techniques, means that liquid-cell electron microscopy can provide information that cannot be obtained using other methods.

Electron microscopy of liquids has developed in two directions, using closed and open liquid cells. These approaches have advantages and challenges for each material and process under study. Here, we describe these techniques and illustrate their use through two important applications. Observation of particle nucleation and growth, achieved in closed liquid cells, provides wide opportunities for answering key questions related to liquid-phase synthesis and materials design. Observation of electrochemical processes, which can be achieved in both open and closed cells, illuminates the different capabilities of the two approaches. Based on these and other examples, we assess the future role that electron microscopy of liquid samples will play in an increasingly diverse set of areas in materials science.

Design considerations for electron microscopy of liquids

Closed cells

Water, the most interesting of liquids, has traditionally been incompatible with the vacuum constraints of electron microscopy because of its high vapor pressure. Liquids with high vapor pressure can be separated from the microscope vacuum in a closed liquid cell. This is an enclosure that is filled, sealed, and loaded into the microscope on a sample holder.

Chong-Min Wang, Pacific Northwest National Laboratory, USA; chongmin.wang@pnnl.gov
Hong-Gang Liao, Materials Sciences Division, Lawrence Berkeley National Laboratory, USA; hgliao@lbl.gov
Frances M. Ross, IBM T.J. Watson Research Center, USA; fmross@us.ibm.com
DOI: 10.1557/mrs.2014.283

© 2015 Materials Research Society
https://doi.org/10.1557/mrs.2014.283 Published online by Cambridge University Press

Imaging requires robust, electron-transparent windows that are separated by a controlled, narrow distance, since good image resolution is obtained only through liquid layers thinner than a few micrometers. Although closed cells were considered early in the development of electron microscopy (see the review in Reference 26), development of a practical closed cell required the use of silicon microfabrication techniques.[14] Cells are typically built from two silicon wafers, each of which is coated with a 50–100-nm-thick silicon nitride layer (**Figure 1**a). A region of Si ~100 μm across is etched out of each wafer, forming windows of silicon nitride. A spacer material, such as silicon dioxide patterned onto one wafer, keeps the windows at the correct separation.

Additional functionality can be applied to this basic closed cell. Electrodes can be patterned on the interior surface of the windows and controlled by an external potentiostat to drive electrochemical processes.[14] The interior surfaces can be modified to react with molecules in solution.[27] Liquids can be pumped through the cell[28] to examine mixing or to change the solution chemistry during imaging. More recently, heating and cooling capabilities have allowed observations of phase transformations[29] and crystal growth.[30]

Silicon nitride is strong, relatively inert, and amorphous, an almost ideal window material. However, its presence reduces image resolution. Deflection of the windows by the pressure difference between the liquid within the cell and the vacuum within the microscope decreases the resolution still further,[26,31–36] as the liquid layer can typically be several times thicker[37] in the center of the window compared to the edge. Strategies to improve resolution include the use of thicker, stiffer windows that deflect less and are patterned with small, thinner areas for imaging;[38] posts connecting the windows to reduce window deflection;[39] narrow channels;[40] and graphene as the ultimate window material to enclose small droplets of liquid.[41]

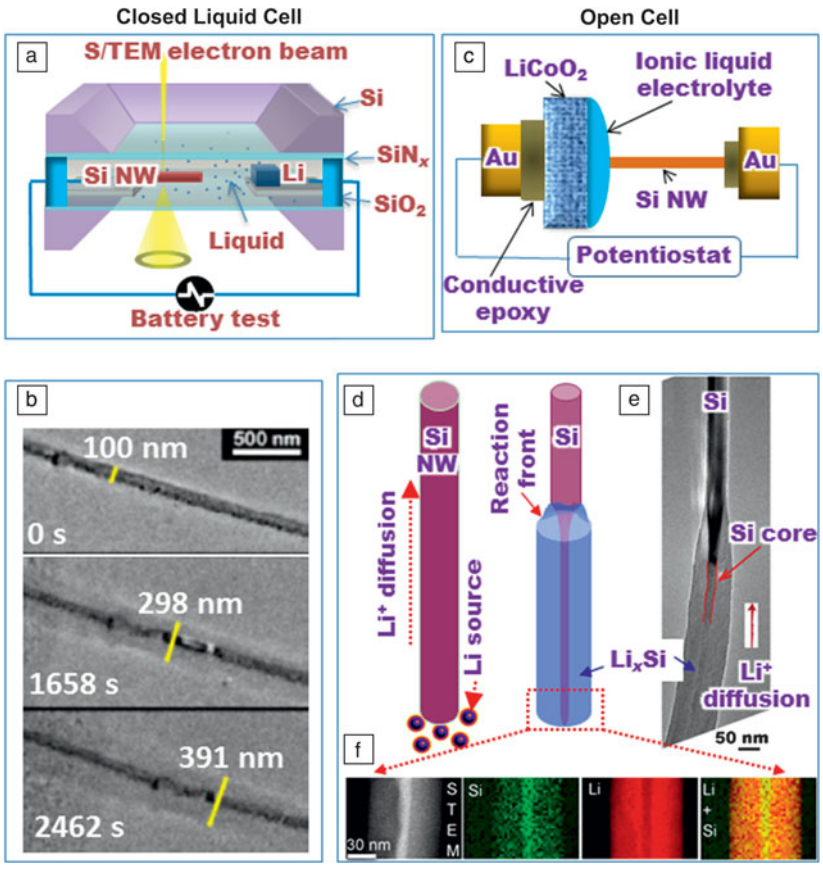


Figure 1. (a) Schematic diagram showing a closed liquid cell with two electrodes, on each of which is attached one component of a battery. The cathode is a Si nanowire (NW), and the anode is metallic Li. (b) Series of images during the lithiation of a crystalline Si NW (in this case coated with Cu to increase conductivity), performed by holding the Cu–Si voltage at ~0.03 V. (c) Schematic diagram showing an open liquid cell with an ionic liquid electrode. (d) Two schematics and (e) an image recorded at a constant voltage of –2 V versus Li metal during lithiation of an (uncoated) Si NW showing the sequential nature of the process. (f) Scanning transmission electron microscopy (STEM) image and electron energy-loss spectroscopy map of element distribution of the process depicted in (d) and (e). (b) and (f) Reproduced with permission from Reference 16. © 2013 American Chemical Society.

Once a closed liquid cell is assembled on its sample holder with the liquid placed or flowed into the cell, the system is tested for leaks and then loaded into the microscope. Many processes of interest, such as liquid-phase particle growth, are driven by the electron beam through its radiolytic effects on the liquid. We present an example of such an experiment later in this article and discuss electron beam effects. Experiments involving electrochemical processes have more complex requirements (Figure 1a). Diffusion often dominates electrochemical behavior, so the need to set up a "realistic" electrochemical process (where thicker liquid layers allow diffusion fields that are more representative of the bulk process) conflicts with the requirements for high image resolution. However, with appropriate cell design, one can observe and quantify nucleation and growth on and around an electrode or at a sample placed on the electrode. We show some electrochemical results later in this article.

The closed liquid cell is a versatile tool for imaging structures and processes in liquids. The main challenge is to optimize resolution while controlling the liquid environment: thickness, flow, electrical bias, and temperature. Closed cells provide the opportunity to set up processes in a liquid film of well-characterized geometry, with the key advantage of being able to observe liquids with high vapor pressure and flowing liquids.

Open cells

For liquids with low vapor pressure, an alternative approach is possible that avoids the decrease in resolution caused by the windows

https://doi.org/10.1557/mrs.2014.283 Published online by Cambridge University Press

in a closed liquid cell. In this case, droplets of liquids, particularly ionic liquids (ILs), are placed directly onto a supporting sample that includes a large-area electrode, and this sample is loaded into the microscope on a custom sample holder. The liquid is stable under vacuum, and electrons can pass through the liquid in regions where it is thin (for example, where it forms a wetting layer ~100 nm in thickness or near the edges of droplets). To examine processes in such free-standing liquid droplets, an electron-transparent probe such as a nanowire is pushed into the liquid, and an electrical bias is applied to drive reactions mediated by the liquid.

Wang et al.[42] and Huang et al.[43] initiated this open cell concept to study reactions in battery materials (Figure 1c). The battery is composed of an ionic liquid electrolyte, a single nanowire electrode, and bulk $LiCoO_2$ as the counter electrode. A typical IL electrolyte is 10% lithium bis(trifluoromethane sulfonyl)imide (LiTFSI) dissolved in a hydrophobic ionic liquid, 1-butyl-1-methylpyrrolidium (P_{14}) TFSI (P_{14}TFSI). The IL wets the nanowire, forming a thin layer around it. Therefore, this configuration mimics a real battery to the extent that the electrolyte conformally coats the active component in the electrode. Open cells offer the possibility of atomic-level spatial resolution and analytical capability for studying the mechanisms of Li-ion insertion into electrode materials during charge/discharge cycles (Figure 1d–f). This has helped reveal details of the lithiation mechanism and structural evolution, especially in anode materials such as Si,[44] Ge,[45] Al_2O_3,[46] SnO_2,[42] ZnO,[47] graphene,[48] and carbon nanotubes.[49] A variation of this experiment uses lithium oxide as the electrolyte rather than an IL. In this configuration, Li metal is used as the anode, and a single nanowire is used as the cathode, with a Li_2O coating on the Li metal surface serving as the electrolyte.[44,50,51] In principle, this is a charged battery that should discharge when the circuit is completed. However, the low conductivity of Li ions in Li_2O at room temperature prevents current flow.[50] A negative potential of typically 2–4 V must be applied between Si and Li to drive Li^+ ions into Si.

Open-cell experiments have provided useful information on structural and chemical evolution of electrodes upon lithiation/delithiation. However, three typical deficiencies are associated with the open-cell configuration. First, the electrolyte is in only point contact with the electrode. This presumably modifies the diffusion pattern of Li ions in the electrode, such that the results are not necessarily representative of a real battery in which the electrode is fully immersed in the liquid electrolyte. Second, when Li_2O is used as the electrolyte, the large overpotential required might change the kinetics and phase behavior of the solid-state electrode lithiation. Third, the use of IL and Li_2O electrolytes excludes the study of many processes in real electrolytes and operating conditions, such as the interaction between electrolyte and electrode and solid–electrolyte interphase (SEI) formation; furthermore, ILs can polymerize under an electron beam, so the cell can be cycled only a limited number of times, short of the performance required for revealing structural evolution as a battery ages. Studies of one material system in open and closed cells can help address the shortcomings of each cell, as we illustrate later in this article.

Materials applications of liquid-cell electron microscopy

Nanoparticle nucleation and growth kinetics in closed cells

Liquid-cell TEM provides a unique platform for the study of colloidal nanoparticle formation. Through the tracking of single-particle growth trajectories, details of the growth mechanisms have been revealed, including previously unrecognized growth pathways.[10,11,41,52,53] Topics of study have included nanoparticle coalescence or oriented attachment,[11,20,41] growth from monomers,[35,53] shape evolution and control,[11,30,52] and surfactant effects.[52] **Figure 2** shows an example in which the nucleation and propagation of individual facets in a nanoparticle were captured using an advanced single-electron detector (a Gatan K2-IS camera providing 400 images per second) during the formation of Pt nanocubes in a liquid precursor solution containing oleylamine surfactant.[30] Direct observation showed that the surface energy minimization rule breaks down at the nanoscale for colloidal synthesis. Instead, a selective facet-arrested growth mechanism was identified, arising from the mobility difference of the surfactants on the facets.

A diverse set of synthetic approaches exists for colloidal nanocrystals. Nanoparticle synthesis is often driven by heating but can also be stimulated by UV–visible light irradiation,[54] microwave heating,[55,56] electrons,[57,58] x-rays,[59] gamma rays,[60] and ion irradiation.[61] Most liquid-cell studies on nanoparticle synthesis have used the electron beam to reduce metal precursors. Recently, however, heating effects are starting to be examined, with observations of oscillatory particle growth at 180°C.[62] Heating extends the range of synthesis techniques

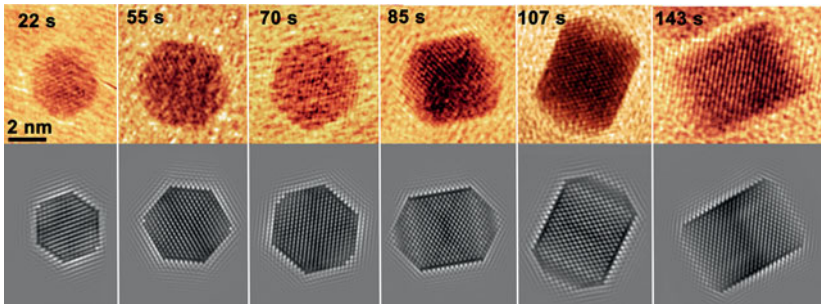


Figure 2. Sequential transmission electron microscope images and corresponding simulated images show the facet development of a Pt nanocube in a liquid cell. A growth solution of platinum bis(acetylacetonate) (20 mg/mL) in a solvent mixture of oleylamine, oleic acid, and pentadecane (4.5:1.5:4) was used. The particles were primarily imaged along the [110] zone axis. Reproduced with permission from Reference 30. © 2014 American Association for the Advancement of Science.

https://doi.org/10.1557/mrs.2014.283 Published online by Cambridge University Press

available for *in situ* observations and suggests that the study of nanocrystal growth using liquid-cell TEM will further enrich the field of colloidal nanocrystals and materials chemistry.

Electrochemical deposition in closed cells

Electrochemical experiments can be carried out in closed cells with great flexibility, as electrodes can be patterned with arbitrary geometry and using a range of materials. **Figure 3**a shows closed-cell data obtained during the nucleation and growth of copper from an acidic copper sulfate electrolyte.[63–65] Copper electro-deposition is used to fabricate conducting tracks in integrated circuits. A continuous yet thin Cu film is required, implying a high initial nucleation density on the polycrystalline liner (the material on which the Cu is deposited). In Figure 3a, Cu growth takes place on polycrystalline Au under conditions of constant voltage. The electrode is transparent to the imaging electrons, allowing the spatial distribution and growth rates of individual Cu islands to be measured. A second key feature of the experiment is the ability to correlate images with the electrochemical response. In Figure 3a, the time-varying current through the whole cell is correlated with the nucleation times and growth rates of the Cu islands. Growth rates, measured from video frames, are then matched with expectations from electrochemical models,[63–65] calculated from the current–time curves, to explore pathways for Cu diffusion and to understand nucleus density. The imaged area is 2 μm^2, while the total electrode area is 2000 μm^2. If we measure the island volumes and hence charge passed for the imaged area and then compare these results with the total charge passed for the total area, the comparison suggests that all areas of the electrode behave uniformly, even those out of view. This type of calibration is important for quantitative analysis of electrochemical processes. Other experiments allow the effects of additives to be examined and the effects of the electron beam to be quantified.[66]

If larger volumes of Cu are grown, the nuclei merge and cover the electrode (Figure 3b), and deposition then proceeds outward from the electrode edge.[18,67] Depending on the growth rate and electrolyte chemistry, such lateral deposition can occur uniformly, or the growth front can become unstable. Instability occurs when growth is controlled by diffusion through the electrolyte, such that random asperities collect more ions and grow even further. Lateral growth experiments provide an interesting model for the charging process in secondary batteries such as those based on Zn or Pb, where nonuniform deposition onto the anode during charging can short the battery. Figure 3b shows the development of an unstable Cu growth front, and Figure 3c shows Pb dendrites grown from lead nitrate,[15] relevant to conventional lead-acid batteries.

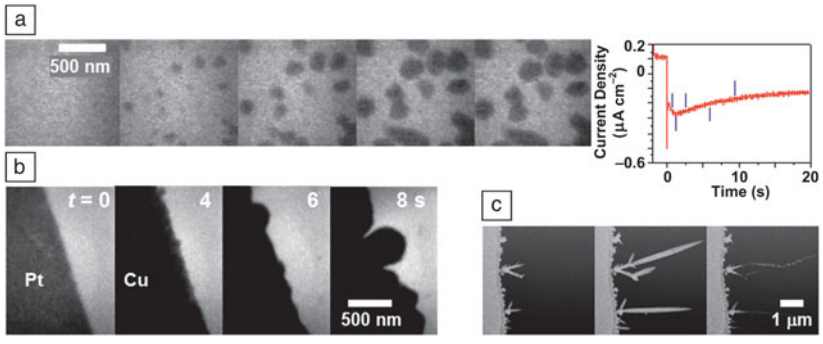


Figure 3. Electrochemical deposition in the liquid cell. (a) Time-varying current recorded during the deposition of Cu on polycrystalline Au from 0.1 M $CuSO_4$ + 1 vol% H_2SO_4 at a potential of –0.07 V, with images extracted from a video recorded simultaneously. The times corresponding to the images are indicated by vertical marks. Nucleation and growth of individual Cu crystallites can be measured. (b) Deposition of Cu onto polycrystalline Pt from the same electrolyte, at –1.2 V relative to the open-circuit potential. Time zero corresponds to application of the potential. Initial rapid coverage of the electrode is followed by unstable lateral growth. The field of view was moved to track the growth front. (c) Pb dendrite growth and collapse from 1.5 M $PbNO_3$ during application of square-wave voltage pulses. (a) Reproduced with permission from Reference 63. © 2006 American Chemical Society. (b) Reproduced with permission from Reference 67. © 2012 Indian Institute of Science. (c) Reproduced with permission from Reference 15. © 2012 American Chemical Society.

Lithium-ion battery anode reactions in closed and open cells

Charge and discharge processes in lithium-ion batteries (LIBs), involving insertion/extraction of ions into/from a host lattice, can be examined in both closed and open cells if the electrolyte has appropriate stability. Figure 1b shows closed-cell results from Gu et al.[16] obtained during lithiation and delithiation of a Si nanowire in a battery-relevant electrolyte; similar devices have been demonstrated by other groups.[16,68–71] It is interesting to compare Figure 1b with nanowire lithiation observed in an open cell, Figure 1e. In the open cell, lithiation proceeds in a sequential manner, and the experiment provides excellent resolution of the structure changes, dislocations, and mechanical deformation that occur during the process. In the closed cell, lithiation and delithiation progress in a core–shell fashion; in other words, the exterior surface of the nanowire reacts first, and more central regions react subsequently. The difference in reaction mechanism can be understood in terms of the diffusion pathways available. In the closed cell, ions arrive from the large volume of electrolyte that surrounds the nanowire, whereas in the open cell, ions diffuse through the thin layer that wets the nanowire. Different reaction interfaces and stress relaxation processes are expected. Thus, comparing results from the two types of liquid cells is the best way to understand the true behavior of the active materials in an LIB electrode.

Lithium-ion battery cathode reactions in closed and open cells

Lithium-ion transport in $LiFePO_4$ serves as the prototypical example to address scientific

https://doi.org/10.1557/mrs.2014.283 Published online by Cambridge University Press

questions related to ion transport in cathode materials. It is known that the removal and insertion of Li ions lead to a reversible phase transformation, $LiFePO_4 \leftrightarrow FePO_4$. Three models have been proposed to describe Li-ion transport, namely, the shrinking-core,[72] phase-boundary migration,[73] and solid-solution[74] models; distinguishing these models requires correlation of ionic transport with structure. **Figure 4** shows Li-ion transport kinetics and degradation mechanisms in $LiFePO_4$ particles during charge/discharge cycles[68] obtained in a closed cell using energy-filtered TEM imaging. A valence energy loss peak at 5 eV was selected because it is unique for $FePO_4$ but not $LiFePO_4$. This allows determination of the lithiation state of a $LiFePO_4$ electrode and the surrounding aqueous electrolyte in real time and nanoscale resolution during electrochemical charge and discharge. In Figure 4, delithiation occurs particle-by-particle, with slow nucleation and growth starting at the edge and moving through each particle. This behavior supports an anisotropic growth model. Open-cell results[75] are consistent with this model in that many of the particles appear inactive at any moment. Li enrichment and depletion captured during lithiation and delithiation highlight the advantages of nanoscale imaging under *operando* conditions.

Solid–electrolyte interphase formation in closed cells

The complex reactions occurring at the electrode–electrolyte interface lead to the formation of a passive layer, SEI, at the electrode surface.[76] The SEI is fundamental to battery performance and lifetime because it controls the passivation, stability, and impedance of the electrode. The chemistry and evolution of the SEI with cycling are therefore key topics for liquid-cell studies. Two recent closed-cell reports highlighted several aspects of SEI formation. During electrochemical lithiation and delithiation of Au anodes in $LiPF_6$/ethylene carbonate (EC)/diethyl carbonate electrolyte,[70] lithiation occurs inhomogeneously, showing lithium metal dendritic growth, electrolyte decomposition, and SEI formation during cyclic voltammetry. The SEI layer develops uniformly on one Au electrode, concurrently with Li dendrite growth on the other electrode. In another observation using $LiPF_6$/EC/dimethyl carbonate,[69] a dendritic SEI appeared on an Au electrode, forming prior to Li deposition and remaining after Li dissolution. Neither of these studies included a lithium metal source; thus, all of the phenomena observed were the result of electrolyte decomposition. Experiments that use a Li source and a reference electrode would provide a systematic and quantitative set of data addressing the key questions of SEI formation kinetics and stability.

Electron beam effects

In any electron microscopy experiment, the modification of the sample by the imaging electrons must be understood and taken into account before one can draw conclusions about the mechanism of the process under study. For solid samples, the effects of high-energy electrons have been studied in detail both theoretically and experimentally.[64–66,77] Electron beam-induced damage is minimized by adjusting the accelerating voltage or reducing the electron dose to as low a level as practical. For liquids, damage mechanisms are somewhat different because of the differences in bonding and in the diffusion and reaction pathways available for the beam-induced products. High-energy electrons generate primary and secondary radiolysis products. These products rapidly (within seconds) reach equilibrium concentrations in the region irradiated by the electron beam.[67] In the radiolysis of pure water, one product is hydrogen gas, which can produce bubbles if its steady-state concentration is above the solubility limit.[67] Another product is hydrogen ions; thus, the electron beam can change the pH of a solution under study, which can, of course, alter the stability of other species in solution. A third highly reactive product is the hydrated (or solvated) electron. This species is thought to be responsible for the reduction of metallic cations in aqueous salt solutions, leading to the phenomena observed in experiments that measure beam-induced growth of metallic nanoparticles[78,79] and beam effects during electrochemical deposition.[67]

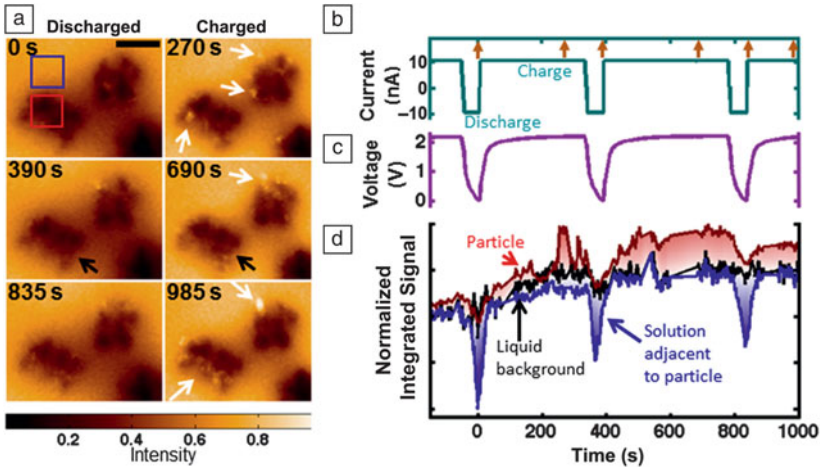


Figure 4. Energy-filtered transmission electron microscopy (EFTEM) data showing structural and chemical evolution of a $LiFePO_4$ cathode, with an activated carbon counter electrode and an aqueous 0.5 M Li_2SO_4 electrolyte. (a) EFTEM images (5 eV) of charging and discharging at indicated times. Scale bar = 400 nm. Bright regions are delithiated $FePO_4$, and dark regions are $LiFePO_4$. White arrows point toward "bright" charged particles, and black arrows point toward "dark" discharged particles. (b) Current profile corresponding to a charge rate of 10 C. Time t = 0 s is the start of the third charge cycle after assembly. Arrows on the top axis indicate the times of the images in (a). (c–d) Integrated intensity over various regions, shown as voltage, from the regions indicated by boxes in (a). The solution becomes dark during discharge and returns to the background level during charge. Regions of the particle light up and disappear, potentially upon delithiating and fracturing off the particle cluster. Reproduced with permission from Reference 68. © 2014 American Chemical Society.

https://doi.org/10.1557/mrs.2014.283 Published online by Cambridge University Press

In more complex, nonaqueous solutions, such as the electrolytes of interest for LIBs, the solvated electrons and other radical species formed can interact chemically with the salt and solvent. It has been suggested[80] that the effect of the electron beam on an electrolyte can provide information on the degradation mechanism of that electrolyte when used in a battery. Breakdown under the beam causes localized electrochemical reactions, whose extent correlates with stability as measured though electrochemical testing. This suggests that electron microscopy can provide insights into the reduction/degradation processes that take place during the operation of LIBs.

Summary and perspective

Imaging in a liquid environment by transmission electron microscopy and scanning transmission electron microscopy provides unique new information in several active scientific areas. In this article, we have highlighted two materials science applications: nanoparticle nucleation and growth, and kinetics during electrodeposition and battery operation. Other active areas include biological structures and processes, biomineralization, bubble and droplet dynamics, aggregation and self-assembly, corrosion, radiation physics, and geological processes.

In the two areas discussed in detail, future developments in liquid-cell microscopy technique can hopefully provide additional information. For nanoparticle nucleation and growth, improvements in liquid cell design, camera speed, and image resolution will increase the level of accessible detail. In addition, the ability to control the liquid temperature will help to expand the phenomena under study beyond those induced by the beam. For battery processes, it is generally hoped that a critical contribution of the closed cell will be a better understanding of solid-electrolyte interphase formation. Achieving this will require an understanding of beam-induced effects on the electrolyte, as well as how to minimize them by reducing the dose.[31,33] It will also require that resolution be improved by reducing the window and liquid thickness, but without making the liquid layer so thin that diffusion pathways are altered. Finally, a challenge remains in constructing a device that can be cycled long enough to allow SEI formation and probe degradation mechanisms. A combination of closed- and open-cell experiments using imaging and analytical electron microscopy provides the best pathway toward obtaining some understanding of the key phenomena at work during battery operation as well as more general electrochemical processes.

Extending the applications of liquid-cell microscopy still further, for example, to areas such as electrocatalysis and yet more complex electrochemical and nanoparticle systems, requires critical enhancement of the resolution and analytical capabilities of the electron microscope. Further opportunities will arise, given capabilities such as temperature control, mixing of two or more components (liquid or gas), and the ability to include stimuli such as visible or ultraviolet light. These and other areas under development suggest an exciting future for liquid-cell electron microscopy in materials science and biology.

Acknowledgments

C.-M.W. acknowledges the support of the Assistant Secretary for Energy Efficiency and Renewable Energy, Office of Vehicle Technologies, of the US Department of Energy (DOE) under Contract DE-AC02-05CH11231, Subcontract 18769, under the Batteries for Advanced Transportation Technologies program. The *in situ* TEM capability is developed under the Chemical Imaging Initiative at Pacific Northwest National Laboratory (PNNL). C.-M.W. also acknowledges the support of the William R. Wiley Environmental Molecular Sciences Laboratory, a national scientific user facility sponsored by DOE's Office of Biological and Environmental Research and located at PNNL. PNNL is operated by Battelle for the DOE under Contract DE-AC05-76RL01830. H.-G.L. was supported by the DOE Office of Science Early Career Research Program under the supervision of Dr. Zheng at Lawrence Berkeley National Laboratory (LBNL). H.-G.L. also acknowledges the facility support of the National Center for Electron Microscopy at LBNL, which is supported by the Office of Basic Energy Sciences, Division of Materials Sciences and Engineering, of the US DOE under Contract DE-AC02-05CH11231.

References

1. M. Haider, S. Uhlemann, E. Schwan, H. Rose, B. Kabius, K. Urban, *Nature* **392** (6678), 768 (1998).
2. K.W. Urban, *Nat. Mater.* **8**, 260 (2009).
3. D.A. Muller, *Nat. Mater.* **8**, 263 (2009).
4. A.R. Harutyunyan, G.G. Chen, T.M. Paronyan, E.M. Pigos, O.A. Kuznetsov, K. Hewaparakrama, S.M. Kim, D. Zakharov, E.A. Stach, G.U. Sumanasekera, *Science* **326** (5949), 116 (2009).
5. B.J. Kim, J. Tersoff, S. Kodambaka, M.C. Reuter, E.A. Stach, F.M. Ross, *Science* **322** (5904), 1070 (2008).
6. P.L. Hansen, J.B. Wagner, S. Helveg, J.R. Rostrup-Nielsen, B.S. Clausen, H. Topsøe, *Science* **295** (5562), 2053 (2002).
7. P. Nolte, A. Stierle, N.Y. Jin-Phillipp, N. Kasper, T.U. Schulli, H. Dosch, *Science* **321**, 1654 (2008).
8. H. Yoshida, Y. Kuwauchi, J.R. Jinschek, K. Sun, S. Tanaka, M. Kohyama, S. Shimada, M. Haruta, S. Takeda, *Science* **335**, 317 (2012).
9. A.M. Minor, S.A.S. Asif, Z.W. Shan, E.A. Stach, E. Cyrankowski, T.J. Wyrobek, O.L. Warren, *Nat. Mater.* **5** (9), 697 (2006).
10. H.M. Zheng, R.K. Smith, Y.W. Jun, C. Kisielowski, U. Dahmen, A.P. Alivisatos, *Science* **324** (5932), 1309 (2009).
11. H.-G. Liao, L.K. Cui, S. Whitelam, H.M. Zheng, *Science* **336** (6084), 1011 (2012).
12. J.E. Evans, K.L. Jungjohann, N.D. Browning, I. Arslan, *Nano Lett.* **11** (7), 2809 (2011).
13. H.M. Zheng, S.A. Claridge, A.M. Minor, A.P. Alivisatos, U. Dahmen, *Nano Lett.* **9** (6), 2460 (2009).
14. M.J. Williamson, R.M. Tromp, P.M. Vereecken, R. Hull, F.M. Ross, *Nat. Mater.* **2** (8), 532 (2003).
15. E.R. White, S.B. Singer, V. Augustyn, W.A. Hubbard, M. Mecklenburg, B. Dunn, B.C. Regan, *ACS Nano* **6** (7), 6308 (2012).
16. M. Gu, L.R. Parent, B.L. Mehdi, R.R. Unocic, M.T. McDowell, R.L. Sacci, W. Xu, J.G. Connell, P. Xu, P. Abellan, X. Chen, Y. Zhang, D.E. Perea, J.E. Evans, L.J. Lauhon, J.-G. Zhang, J. Liu, N.D. Browning, Y. Cui, I. Arslan, C.-M. Wang, *Nano Lett.* **13** (12), 6106 (2013).
17. X. Chen, K.W. Noh, J.G. Wen, S.J. Dillon, *Acta Mater.* **60**, 192 (2012).
18. U. Mirsaidov, C.-D. Ohl, P. Matsudaira, *Soft Matter* **8**, 7108 (2012).
19. E.R. White, M. Mecklenburg, S.B. Singer, S. Aloni, B.C. Regan, *Appl. Phys. Express* **4**, 055201 (2011).
20. D. Li, M.H. Nielsen, J.R. Lee, C. Frandsen, J.F. Banfield, J.J. De Yoreo, *Science* **336** (6084), 1014 (2012).

https://doi.org/10.1557/mrs.2014.283 Published online by Cambridge University Press

21. T.W. Huang, S.Y. Liu, Y.J. Chuang, H.Y. Hsieh, C.Y. Tsai, W.J. Wu, C.T. Tsai, U. Mirsaidov, P. Matsudaira, C.S. Chang, F.G. Tseng, F.R. Chen, *Soft Matter* **9** (37), 8856 (2013).
22. M.T. Proetto, A.M. Rush, M.-P. Chien, P. Abellan Baeza, J.P. Patterson, M.P. Thompson, N.H. Olson, C.E. Moore, A.L. Rheingold, C. Andolina, J. Millstone, S.B. Howell, N.D. Browning, J.E. Evans, N.C. Gianneschi, *J. Am. Chem. Soc.* **136** (4), 1162 (2014).
23. N. de Jonge, D.B. Peckys, G.J. Kremers, D.W. Piston, *Proc. Natl. Acad. Sci. U.S.A.* **106** (7), 2159 (2009).
24. U.M. Mirsaidov, H.M. Zheng, Y. Casana, P. Matsudaira, *Biophys. J.* **102** (4), L15 (2012).
25. J.E. Evans, K.L. Jungjohann, P.C.K. Wong, P.-L. Chiu, G.H. Dutrow, I. Arslan, N.D. Browning, *Micron* **43** (11), 1085 (2012).
26. N. de Jonge, F.M. Ross, *Nat. Nano technol.* **6** (11), 695 (2011).
27. K. Degen, M. Dukes, J.R. Tanner, D.F. Kelly, *RSC Adv.* **2**, 2408 (2012).
28. E.A. Ring, N. de Jonge, *Microsc. Microanal.* **16**, 622 (2010).
29. K. Tai, Y. Liu, S.J. Dillon, *Microsc. Microanal.* **20**, 330 (2014).
30. H.-G. Liao, D. Zherebetskyy, H.L. Xin, C. Czarnik, P. Ercius, H. Elmlund, M. Pan, L.W. Wang, H.M. Zheng, *Science* **345** (6199), 916 (2014).
31. T.J. Woehl, K.L. Jungjohann, J.E. Evans, I. Arslan, W.D. Ristenpart, N.D. Browning, *Ultramicroscopy* **127**, 53 (2013).
32. K.L. Jungjohann, J.E. Evans, J.A. Aguiar, I. Arslan, N.D. Browning, *Microsc. Microanal.* **18** (03), 621 (2012).
33. R.F. Egerton, *Ultramicroscopy* **127**, 100 (2013).
34. N. de Jonge, D.B. Peckys, G.J. Kremers, D.W. Piston, *Proc. Natl. Acad. Sci. U.S.A.* **106**, 2159 (2009).
35. T.J. Woehl, J.E. Evans, I. Arslan, W.D. Ristenpart, N.D. Browning, *ACS Nano* **6** (10), 8599 (2012).
36. D.A. Welch, R. Faller, J.E. Evans, N.D. Browning, *Ultramicroscopy* **135**, 36 (2013).
37. K.L. Jungjohann, J.E. Evans, J.A. Aguiar, I. Arslan, N.D. Browning, *Microsc. Microanal.* **18** (3), 621 (2012).
38. J.F. Creemer, S. Helveg, G.H. Hoveling, S. Ullmann, A.M. Molenbroek, P.M. Sarro, H.W. Zandbergen, *Ultramicroscopy* **108**, 993 (2008).
39. J.M. Grogan, H.H. Bau, *J. Microelectromech. Syst.* **19**, 885 (2010).
40. E. Jensen, A. Burrows, K. Mølhave, *Microsc. Microanal.* **20**, 445 (2014).
41. J.M. Yuk, J. Park, P. Ercius, K. Kim, D.J. Hellebusch, M.F. Crommie, J.Y. Lee, A. Zettl, A.P. Alivisatos, *Science* **336** (6077), 61 (2012).
42. C.M. Wang, W. Xu, J. Liu, D.W. Choi, B. Arey, L.V. Saraf, J.G. Zhang, Z.G. Yang, S. Thevuthasan, D.R. Baer, N. Salmon, *J. Mater. Res.* **25**, 1541 (2010).
43. J.Y. Huang, L. Zhong, C.M. Wang, J.P. Sullivan, W. Xu, L.Q. Zhang, S.X. Mao, N.S. Hudak, X.H. Liu, A. Subramanian, H. Fan, L. Qi, A. Kushima, J. Li, *Science* **330** (6010), 1515 (2010).
44. X.H. Liu, H. Zheng, L. Zhong, S. Huang, K. Karki, L.Q. Zhang, Y. Liu, A. Kushima, W.T. Liang, J.W. Wang, J.-H. Cho, E. Epstein, S.A. Dayeh, S.T. Picraux, T. Zhu, J. Li, J.P. Sullivan, J. Cumings, C.-M. Wang, S.X. Mao, Z.Z. Ye, S. Zhang, J.Y. Huang, *Nano Lett.* **11** (8), 3312 (2011).
45. X.H. Liu, S. Huang, S.T. Picraux, J. Li, T. Zhu, J.Y. Huang, *Nano Lett.* **11** (9), 3991 (2011).
46. Y. Liu, N.S. Hudak, D.L. Huber, S.J. Limmer, J.P. Sullivan, J.Y. Huang, *Nano Lett.* **11** (10), 4188 (2011).
47. A. Kushima, X.H. Liu, G. Zhu, Z.L. Wang, J.Y. Huang, J. Li, *Nano Lett.* **11**, (11), 4535 (2011).
48. X.H. Liu, J.W. Wang, Y. Liu, H. Zheng, A. Kushima, S. Huang, T. Zhu, S.X. Mao, J. Li, S. Zhang, W. Lu, J.M. Tour, J.Y. Huang, *Carbon* **50** (10), 3836 (2012).
49. Y. Liu, H. Zheng, X.H. Liu, S. Huang, T. Zhu, J. Wang, A. Kushima, N.S. Hudak, X. Huang, S. Zhang, S.X. Mao, X. Qian, J. Li, J.Y. Huang, *ACS Nano* **5** (9), 7245 (2011).
50. M.M. Islam, T. Bredow, *J. Phys. Chem. C* **113**, 672 (2009).
51. F. Wang, H.-C. Yu, M.-H. Chen, L. Wu, N. Pereira, K. Thornton, A. Van der Ven, Y. Zhu, G.G. Amatucci, J. Graetz, *Nat. Commun.* **3**, 1201 (2012).
52. H.-G. Liao, H. Zheng, *J. Am. Chem. Soc.* **135** (13), 5038 (2013).
53. K.L. Jungjohann, S. Bliznakov, P.W. Sutter, E.A. Stach, E.A. Sutter, *Nano Lett.* **13** (6), 2964 (2013).
54. O. Akhavan, E. Ghaderi, *J. Phys. Chem. C* **113** (47), 20214 (2009).
55. A.B. Panda, G. Glaspell, M.S. El-Shall, *J. Am. Chem. Soc.* **128** (9), 2790 (2006).
56. X.-H. Liao, N.-Y. Chen, S. Xu, S.-B. Yang, J.-J. Zhu, *J. Cryst. Growth* **252**, (4), 593 (2003).
57. Z. Li, L. Peng, Y. Fang, Z. Chen, D. Pan, M. Wu, *Radiat. Phys. Chem.* **80**, (12), 1333 (2011).
58. F. Zhou, R. Zhou, X. Hao, X. Wu, W. Rao, Y. Chen, D. Gao, *Radiat. Phys. Chem.* **77** (2), 169 (2008).
59. R. Divan, Q. Ma, D. Mancini, D. Keane, *Rom. J. Inf. Sci. Technol.* **11** (1), 71 (2008).
60. J. Rojas, C. Castano, *Radiat. Phys. Chem.* **81** (1), 16 (2012).
61. Y. Mishra, D. Avasthi, P. Kulriya, F. Singh, D. Kabiraj, A. Tripathi, J. Pivin, I. Bayer, A. Biswas, *Appl. Phys. Lett.* **90** (7), 073110 (2007).
62. H.L. Xin, H. Zheng, *Nano Lett.* **12** (3), 1470 (2012).
63. A. Radisic, P.M. Vereecken, J.B. Hannon, P.C. Searson, F.M. Ross, *Nano Lett.* **6**, 238 (2006).
64. A. Radisic, F.M. Ross, P.C. Searson, *J. Phys. Chem. B* **110**, 7862 (2006).
65. A. Radisic, P.M. Vereecken, P.C. Searson, F.M. Ross, *Surf. Sci.* **600**, 1817 (2006).
66. M. den Heijer, I. Shao, A. Radisic, M.C. Reuter, F.M. Ross, *APL Mater.* **2**, 022101 (2014).
67. J.M. Grogan, N.M. Schneider, F.M. Ross, H.H. Bau, *J. Indian Inst. Sci.* **92**, 295 (2012).
68. M.E. Holtz, Y. Yu, D. Gunceler, J. Gao, R. Sundararaman, K.A. Schwarz, T.S.A. Arias, H.C.D. Abruña, D.A. Muller, *Nano Lett.* **14**, 1453 (2014).
69. R.L. Sacci, N.J. Dudney, K.L. More, L.R. Parent, I. Arslan, N.D. Browning, R.R. Unocic, *Chem. Commun.* **50**, 2104 (2014).
70. Z. Zeng, W.-I. Liang, H.-G. Liao, H.L. Xin, Y.-H. Chu, H. Zheng, *Nano Lett.* **14**, 1745 (2014).
71. R.R. Unocic, R.L. Sacci, G.M. Brown, G.M. Veith, N.J. Dudney, K.L. More, F.S. Walden II, D.S. Gardiner, J. Damiano, D.P. Nackashi, *Microsc. Microanal.* **20**, 452 (2014).
72. D. Morgan, A. Van der Ven, G. Ceder, *Electrochem. Solid-State Lett.* **7** (2), A30–A32 (2004).
73. P. Gibot, M. Casas-Cabanas, L. Laffont, S. Levasseur, P. Carlach, S. Hamelet, J.M. Tarascon, C. Masquelierk, *Nat. Mater.* **7** (9), 741 (2008).
74. R. Malik, F. Zhou, G. Ceder, *Nat. Mater.* **10** (8), 587 (2011).
75. Y. Zhu, J.W. Wang, Y. Liu, X. Liu, A. Kushima, Y. Liu, Y. Xu, S.X. Mao, J. Li, C. Wang, J.Y. Huang, *Adv. Mater.* **25**, 5461 (2013).
76. K. Kang Xu, A. von Cresce, U. Lee, *Langmuir* **26** (13), 11538 (2010).
77. J.M. Grogan, N.M. Schneider, F.M. Ross, H.H. Bau, *Nano Lett.* **14**, 359 (2014).
78. J. Belloni, M. Mostafavi, H. Remita, J.L. Marignier, M.O. Delcourt, *New J. Chem.* **22** (11), 1239 (1998).
79. J. Belloni, *Catal. Today* **113** (3–4), 141 (2006).
80. P. Abellan, B.L. Mehdi, L.R. Parent, M. Gu, C. Park, W. Xu, Y. Zhang, I. Arslan, J.-G. Zhang, C.-M. Wang, J.E. Evans, N.D. Browning, *Nano Lett.* **14**, 1293 (2014). □

JANIS

Cryogenic Wafer Probe Stations



- Applications include nano science, materials and spintronics
- 3.2 K - 675 K; high vacuum or UHV
- Up to 8 probes, DC to 67 GHz, plus fiber optics
- Zoom optics with camera and monitor
- Cooling options: liquid helium, liquid nitrogen or cryogen free
- Horizontal, vertical or vector magnetic field options are available

Contact us today:
sales@janis.com
www.janis.com/ProbeStations.aspx
www.facebook.com/JanisResearch

https://doi.org/10.1557/mrs.2014.283 Published online by Cambridge University Press